Bulletin of the Seismological Society of America, Vol. 104, No. 1, pp. 321–335, February 2014, doi: 10.1785/0120130116

Earthquake Ground Motion and 3D Georgia Basin Amplification in Southwest British Columbia: Shallow Blind-Thrust Scenario Earthquakes

by Sheri Molnar,* John F. Cassidy,† Kim B. Olsen, Stan E. Dosso, and Jiangheng He

Abstract Finite-difference modeling of 3D long-period (> 2 s) ground motions for large (M_w 6.8) scenario earthquakes is conducted to investigate the effects of the Georgia basin structure on ground shaking in Greater Vancouver, British Columbia, Canada. Scenario earthquakes include shallow blind-thrust North America (NA) plate earthquakes, simulated in locations congruent with linear clusters of shallow seismicity, that is, potential active faults. A slip distribution model of the M_w 6.7 Northridge, California, blind-thrust earthquake, with the hypocenter modified to 5 km depth, is used to characterize the source rupture process. Two sets of simulations are performed for a given scenario earthquake using models with and without Georgia basin sediments. The ratio of predicted peak ground velocity (PGV) for the two simulations is applied here as a quantitative measure of amplification due to 3D basin structure. A total of eight shallow blind-thrust NA plate scenario earthquakes are simulated within 100 km of Greater Vancouver. Overall, predicted ground motions are higher in the down-dip direction of each epicenter due to the source radiation pattern; hence, scenario earthquakes located south of Vancouver produce the highest motions in the city. The average maximum PGV at stiff soil sites across Greater Vancouver considering all eight scenario earthquakes is 17.8 cm/s (modified Mercalli intensity VII); the average increase in peak motion due to the presence of Georgia basin sediments is a factor of 4.1. The effective duration of moderate-level (≥ 3.4 cm/s) shaking within Greater Vancouver is an average of 22 s longer when Georgia basin sediments are included in the 3D structure model.

Online Material: Snapshots and videos of wave propagation, and peak ground velocity maps.

Introduction

This paper presents finite-difference (FD) simulations of long-period (> 2 s) ground motions computed for M_w 6.8 shallow North America (NA) plate scenario earthquakes in southwest British Columbia in a regional 3D velocity model of the Georgia basin; Molnar *et al.* (2014), deals with deep (42–55 km) subducting Juan de Fuca (JdF) plate scenario earthquakes. The main objective in this study and in Molnar *et al.* (2014), is to examine the effect of 3D Georgia basin structure on predicted ground shaking across Greater Vancouver from large (M_w 6.8) scenario earthquakes.

Greater Vancouver is located in southwest British Columbia, Canada, and the area of highest seismic risk in Canada. Here, a population of over 2 million and critical infrastructure are located at the northern end of the active Cascadia subduction zone where the oceanic JdF plate subducts in a northeast direction beneath the continental NA plate. Earthquakes occur within the NA crust in response to compression; the activity rate of M_w 5 NA plate events per year spanning from southern Puget Sound, Washington, to Vancouver, British Columbia, is approximately one event every 20 years, and the best-estimate maximum magnitude is 7.3 (Adams and Halchuk, 2003). Large (M > 7) historical events in 1872, 1918, and 1946 occurred in Washington and on Vancouver Island, whereas moderate- and small-sized events occur predominantly beneath Georgia Strait (Fig. 1). Recorded seismicity of moderate and small events exhibits a bimodal depth distribution; moderate events in 1939, 1975,

*Also at Natural Resources Canada, P.O. Box 6000, Sidney, British Columbia V8L 4B2; and now at Department of Civil Engineering, University of British Columbia, 6250 Applied Science Lane, Vancouver, British Columbia V6K 1C1; semolnar@mail.ubc.ca.

†Also at School of Earth and Ocean Sciences, University of Victoria, 3800 Finnerty Road, Victoria, British Columbia V8P 5C2.

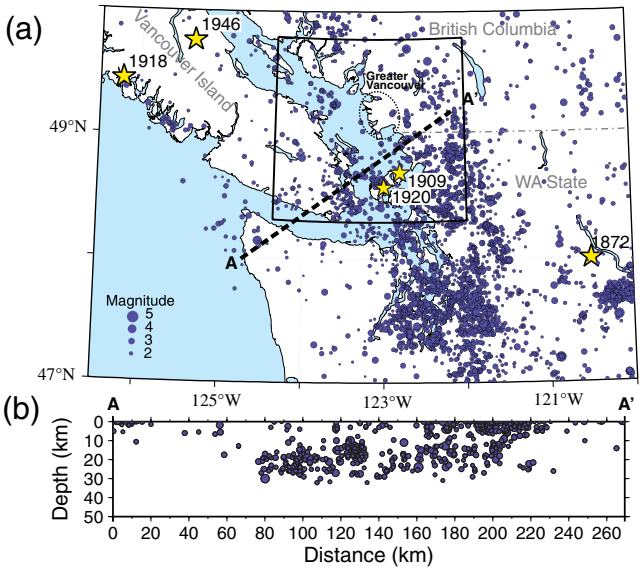

Figure 1. (a) Shallow North America plate seismicity (1985–1999). Significant earthquakes ($M_w \geq 5.5$) are represented by stars and labeled by year. Limits of the Georgia basin regional model are shown by the solid box, the Greater Vancouver region is bounded by the dotted ellipse, and the international border is indicated by the dashed-dotted line. The thick dashed line denotes seismic cross-section A–A′ shown in (b) (M_L 2 minimum). The color version of this figure is available only in the electronic edition.

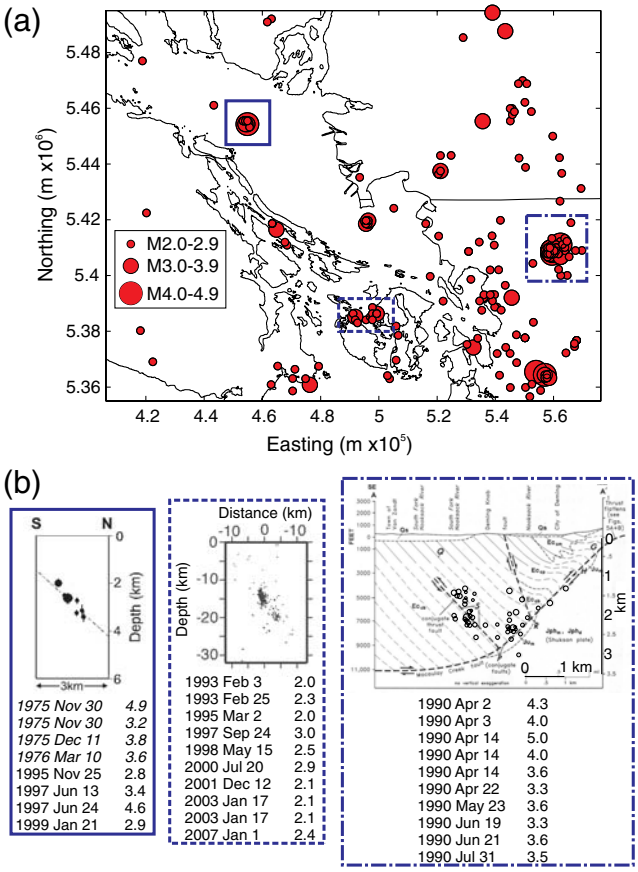

Figure 2. (a) Locations of shallow (≤20 km) seismicity (1985–2012) in the Georgia basin region (filled circles). Three clusters of seismicity are outlined by solid, dashed, and dotted-dashed boxes. (b) Cross-section plots of clustered seismicity and corresponding lists of the largest events (from left to right, modified from Cassidy *et al.*, 2000, Balfour, Cassidy, and Dosso, 2011, and Dragovich *et al.*, 1997, respectively). Italicized events in list are not shown. The color version of this figure is available only in the electronic edition.

1990, 1996, and 1997 occurred at shallow depths (≤7 km) followed by numerous aftershocks, whereas small events are concentrated at depths of 15–25 km. Two moderate-sized events occurred beneath the San Juan Islands, Washington, in 1909 (M 6.0) and 1920 (M 5.5) and are considered crustal NA plate events (<30 km depth) due to several locally felt aftershocks and a short interval between *P*- and *S*-wave arrivals of ~3–4 s, respectively (G. Rogers, personal comm., 2013).

Rupture characteristics of a large crustal NA plate earthquake in southwest British Columbia are virtually unknown because large historical events occurred prior to installation of a local seismic network and no event larger than M 5 has been recorded in the Georgia basin region. The most comprehensive examination of focal mechanism (i.e., fault-plane) solutions from over 1000 M_L <5 NA plate earthquakes shows no dominant style of faulting; ~30% is strike slip, thrust, or some combination thereof (Balfour, Cassidy, *et al.*, 2011). The maximum compressive stress direction from inversion of focal mechanisms is parallel to the Cascadia subduction zone margin, oriented north–south beneath Georgia Strait (Balfour, Cassidy, *et al.*, 2011). Hence, the most likely scenario for a large shallow NA plate earthquake in the Georgia basin region is an approximately east–west striking event that is equally likely to exhibit pure to oblique strike-slip or thrust-faulting behavior.

This paper is focused on potential large blind-thrust shallow NA plate earthquakes in the Georgia basin region; locations and rupture characteristics of scenario earthquakes are based on recurrent shallow seismicity (Fig. 2) and a chosen kinematic rupture model of the 1994 M_w 6.7 Northridge, California, blind-thrust earthquake, respectively. As in Molnar *et al.* (2014), a single source rupture model is used to simulate all scenario earthquakes; hence, the results presented here are limited to the single set of blind-thrust rupture characteristics chosen here. Scenario blind-thrust earthquakes are simulated in different locations in the Georgia basin region, congruent with known seismicity and within 100 km of Vancouver, to investigate variation in the strength of predicted ground motions and 3D basin effects. The finite-difference scheme and 3D physical-structure models are described in Molnar *et al.* (2014). As in Molnar *et al.* (2014), the chosen peak ground velocity (PGV) metric is the geometric mean of the orthogonal horizontal components, calculated as $\max_t(\sqrt{v_{EW}(t) \times v_{NS}(t)})$, in which $v(t)$ represents a synthetic horizontal velocity waveform, EW represents east–west component, and NS represents north–south component. Peak motion values based on the square-root sum of squares of both horizontal and all three components

of motion, termed 2DrssPGV and 3DrssPGV, respectively, are also provided here. The accuracy of the simulations was assessed in Molnar *et al.* (2014) by comparing synthetic and empirical waveforms of the 2001 M_w 6.8 Nisqually earthquake. Amplification due to basin structure is evaluated as the ratio of peak motion from simulations of the same scenario earthquake in 3D basin and nonbasin structure models. As noted in Molnar *et al.* (2014), limitations of this work include: (1) uncertainty in physical-structure and source-rupture models, (2) omission of low-velocity material (e.g., water and up to 300 m of Holocene sediments) and surface topography in the physical-structure models, and (3) inability to resolve frequencies >0.5 Hz. Nonetheless, the work presented here and in Molnar *et al.* (2014) represents an important first step toward quantifying the effect of the 3D sedimentary Georgia basin structure on earthquake ground motion in southwest British Columbia. This research provides the first detailed investigation of 3D earthquake ground motion for a sedimentary basin in Canada.

Physical-Structure Models and Finite-Difference Scheme

Details of the physical-structure models and finite-difference scheme are provided in Molnar *et al.* (2014). A few key points are reiterated here, and details specific to simulations in this paper are provided. The base elastic 3D model is an updated version of the Stephenson (2007) Pacific Northwest 3D velocity model. The physical model is represented by six geologic units characterized by V_P, V_S, and density: continental basin sediments, crust, and mantle; and oceanic sediments, crust, and mantle. Dimensions of the Georgia basin regional model used here are 150 km north–south by 180 km east–west by 25 km vertical. A nonbasin 3D model is also generated from the updated basin model by setting the minimum V_P to 5.5 km/s, effectively replacing basin sediments with inferred basement. The nonbasin velocity model is based on the typical 1D velocity profile for rock sites in southwest British Columbia. For the same scenario earthquake, the ratio of peak motions predicted using the basin and nonbasin models provides a quantitative measure of 3D Georgia basin effects.

The 3D elastic equations of motion are solved here using the FD scheme of Olsen (1994) with fourth-order accuracy in space and second-order accuracy in time. The maximum resolvable frequency is 0.5 Hz (2 s). The minimum V_S is set to 625 m/s; hence, the surface of the 3D basin model represents overconsolidated Pleistocene glacial sediments or stiff soil sites. The Q relations of Frankel *et al.* (2009) for stiff sediments in the Pacific Northwest are the most geologically reasonable and are assigned. Crustal NA plate earthquakes are simulated within 100 km of Greater Vancouver using higher-accuracy harmonic averaging (Olsen, 1994; version 2.6.4) and perfectly matched absorbing boundary layers (Collino and Tsogka, 2001; Marcinkovich and Olsen, 2003). The seismic source is implemented in the FD grid by adding $-M_{ij}(t)/V$ to $S_{ij}(t)$, in which $M_{ij}(t)$ and $S_{ij}(t)$ are the ijth components of the earthquake moment tensor and fault stress tensor at time t, respectively, and V is the cell volume (Olsen, 2000).

Accuracy of the 3D FD simulations is evaluated in Molnar *et al.* (2014) by comparing synthetic and empirical waveforms of the 2001 M_w 6.8 Nisqually earthquake; the bias between predicted and empirical PGV is a factor of 1.6 for 16 selected sites within the Georgia basin.

Earthquake Source Model

The chosen rupture process of the two types of scenario earthquakes is based on actual earthquakes; the 2001 M_w 6.8 Nisqually normal-faulting earthquake is used to simulate deep JdF plate earthquakes and to calibrate predicted motions with observed recordings in Molnar *et al.* (2014), whereas the 1994 M_w 6.7 Northridge blind-thrust earthquake slip distribution of Wald *et al.* (1996) is modified to simulate shallow NA plate scenario earthquakes here. Broadband simulations of shallow California scenario earthquakes via finite-fault kinematic rupture models are strongly influenced by source parameters such as hypocenter, rupture directivity and extent (Aagaard *et al.*, 2008; Harmsen *et al.*, 2008) and less so by small-scale variations in the slip, such as variable rise time and rupture velocity (Aagaard *et al.*, 2010). For example, if rupture velocity is randomly varied between 2.5 and 2.9 km/s, then ground motions change by 50%–300% (Hartzell *et al.*, 2011). In this study, large-scale rupture characteristics (e.g., hypocenter location, rupture style, and direction) are based on observed linear trends of moderate seismicity as described in the Introduction, whereas small-scale rupture characteristics, such as rise time and rupture velocity, are largely unknown and kept relatively simple here. The simulated source wavefield used here does not include spontaneous rupture fluctuations known to occur in reality, which would have the effect of lowering the predicted ground motions (Olsen *et al.*, 2008, 2009).

Table 1 lists the location and source parameter details of the eight scenario earthquakes chosen here. Orientation of the strike and dip direction is generally set to N270°E and 45° N, respectively, unless suggested otherwise by the orientation of the linear clustering of the shallow seismicity upon which the scenario earthquake is based. A 45° dipping fault geometry is chosen for simplicity, which is 5°–15° shallower than observed. The 101° rake angle of the Northridge earthquake is also kept constant in this study.

Following Wald *et al.* (1996), the fault is set to a width of 17.5 km and down-dip length of 24.5 km and is subdivided into 14 subfaults in each direction (Fig. 3b); the fault plane is composed of 196 gridded double-couple point sources. The total seismic moment is set to 1.8×10^{19} N·m, equivalent to an M_w 6.8 event; the same total moment was used for the deep JdF plate scenario earthquakes. Moment release of each subfault is characterized by a half-cosine function (0.5 Hz high-pass filtered) with a constant rise time of 2 s. Generally,

Table 1
Location and Details of Each Scenario Earthquake

Scenario	Name	Distance from Vancouver	Epicenter Latitude (° N)	Epicenter Longitude (° W)	Fault Details	Observed Seismicity
1	Georgia Strait, British Columbia	40 km west	49.2	123.6	N270°E strike 45° dip north	Cassidy *et al.* (2000)
2	Saltspring Island, British Columbia	45 km southwest	48.9	123.4	N300°E strike 45° dip northeast	Shallow cluster
3	Skipjack, Pt. Roberts, British Columbia	50 km south	48.8	123.0	N270°E strike 45° dip north	Shallow cluster
4a	Deming, Washington	80 km east-southeast	48.9	122.2	N90°E strike 45° dip south	Dragovitch *et al.* (1997)
4b	Deming, Washington	80 km east-southeast	48.9	122.1	N240°E strike 45° dip northwest	Dragovitch *et al.* (1997)
5	Victoria, British Columbia	90 km south-southwest	48.5	123.3	N270°E strike 45° dip north	Shallow cluster
6	San Juan Island, Washington	80 km south	48.5	123.0	N270°E strike 45° dip north	Balfour, Cassidy, and Dosso (2011)
7	Mt. Vernon, Washington	110 km south-southeast	48.4	122.2	N270°E strike 45° dip north	Shallow cluster

rise time is short compared with the overall duration (~10%, Heaton, 1990), and a relatively short rise time is characteristic of both the 2005 M_w 7.6 Kashmir, Pakistan, and the 1999 M_w 7.6 Chi-Chi, Taiwan, thrust-mechanism earthquakes and is likely typical of intracontinental events (Avouac *et al.*, 2006). The relation of Sommerville *et al.* (1999) gives a rise time of ~1.3 s for the Northridge event.

Modification of the Northridge slip distribution included flipping (rotation by 180°) the distribution so that larger slip occurs in the near surface rather than at depth, that is, relocation of the 20 km Northridge hypocenter to 5 km depth (Fig. 3b). Slip decreases up-dip of the 5 km hypocenter and reaches zero value at 1.25 km depth, that is, a blind-thrust event. The preferred direction of rupture here is down-dip based on temporal aftershock sequences (Amadi, 1992; Dragovich *et al.*, 1997; Cassidy *et al.*, 2000). A uniform 3.0 km/s rupture velocity is used, as determined for the Northridge event (Wald *et al.*, 1996), which is ~80% of the local V_S (Graves and Pitarka, 2004) in the 3D Georgia basin model used here. Initiation times of each subfault are based on the distance of each subfault center to the hypocenter divided by the uniform 3.0 km/s rupture velocity. Based on the furthest distance, the total duration of the source rupture is 10.3 s.

Previous finite-difference simulation of the Northridge earthquake with a similar approximate kinematic source model reproduces the observed spatial distribution of long-period ground motion, successfully predicts the timing of late-arrival waves, and matches observed PGVs generally within a factor of 2; the simulated PGV of the Northridge earthquake is 22 and 58 cm/s for the two horizontal directions (Olsen and Archuleta 1996). Motion of the north–south (28°) and vertical components is dominant due to source directivity. The Northridge earthquake propagated away from the greater Los Angeles area yet caused an estimated damage loss of U.S. $41.8 billon and was notable due to the collapse of seven major freeway bridges and prevalent damage to soft-story structures (Risk Management Solutions [RMS], 2004).

Scenario Earthquakes

The goal here is to quantify the 3D Georgia basin effect on long-period ground shaking in Greater Vancouver for realistic scenarios of M_w 6.8 shallow NA plate earthquakes. In southwest British Columbia, no obvious correlation exists between mapped surface faults of the Georgia basin region and crustal NA plate earthquakes (Rogers, 1998). Linear clustering of recurrent shallow seismicity indicates potential hidden active faults. One cluster of recurrent shallow (<6 km) seismicity occurs 40 km west of Greater Vancouver (Fig. 2a). A shallow M_L 4.9 thrust earthquake occurred here in 1975 with a long aftershock sequence (Rogers, 1979). In 1997, an M_L 4.6 thrust earthquake at 3–4 km depth also occurred here, accompanied by an M_L 3.4 foreshock and ~53 aftershocks of M_L <2 (Cassidy *et al.* 2000). Relocation of the largest magnitude ($M_L \geq 1.5$) aftershocks delineate a 53° north-dipping trend (Fig. 2b), with a temporal sequence that migrates north (down-dip). A second cluster of recurrent seismicity shown in Figure 2a occurs beneath San Juan Island, Washington, 80 km south of Greater Vancouver. Balfour, Cassidy, and Dosso (2011) performed precise relative relocations of ~300 $M_L \leq 3$ earthquakes (1992–2008) and identified an active structure with a N290°E strike and 60° dip oriented N20°E (Fig. 2b). An east–west strike orientation is determined from focal mechanism solutions, which generally exhibit strike-slip or thrust-faulting behavior, for events of $M_L > 1$ in this area (Balfour, Cassidy, and Dosso, 2011). A third cluster of seismicity shown in Figure 2a is located 80 km east-southeast of Vancouver near Deming, Washington. Here, a swarm of ~1800 shallow (<4 km) earthquakes began on 2 April 1990, with the 10 largest

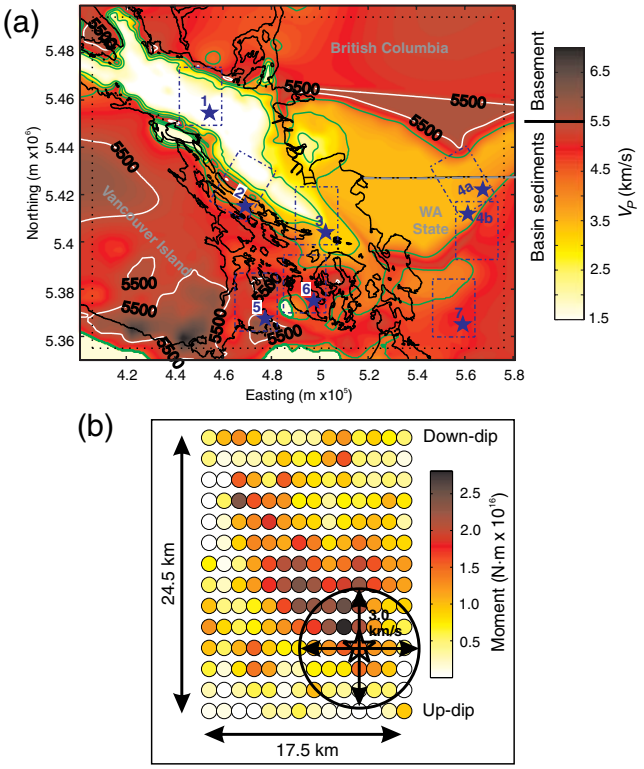

Figure 3. (a) Depth slice of basin V_P model at 500 m depth. The projected fault plane and hypocenter of the eight scenario earthquakes are shown by the dotted-dashed box and star, respectively. The coastline is shown as the thick black line, the international border is the dashed-dotted line, and the 5 km boundary zone is denoted by the dotted line. (b) Each circle corresponds to the location of a subfault; the fill of the circle depends on its associated seismic moment; the hypocenter subfault is denoted by the star and ruptures uniformly at 3.0 km/s. The color version of this figure is available only in the electronic edition.

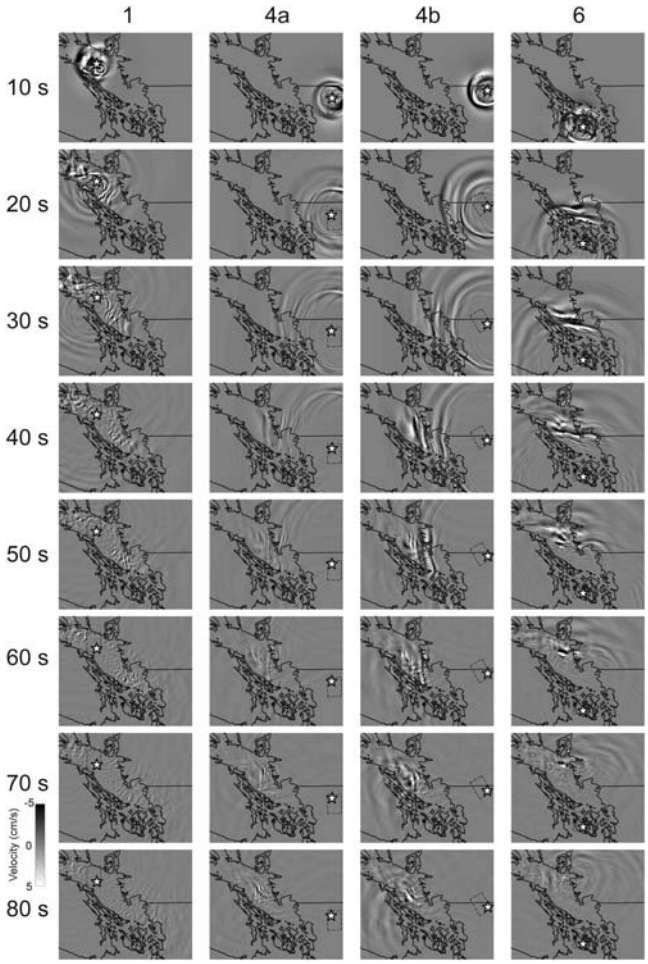

Figure 4. Snapshots of simulated east–west component wave propagation for scenario earthquakes 1, 4a, 4b, and 6 (projected fault plane and hypocenter shown by dotted-dashed box and star, respectively) from 10 to 80 s after the origin time of the rupture; the coastline and the international border are shown by black lines.

events listed in Figure 2b. Earthquakes in all areas of the aftershock zone exhibit thrust faulting; the mainshock and aftershocks during the first four days occurred along a southeast-dipping plane, then aftershocks occurred on a northwest-dipping conjugate backthrust plane (Amadi, 1992; Dragovich *et al.*, 1997). Other apparent clusters of shallow recurrent seismicity outlined in Figure 2a indicate locations of potential active faulting, which are used to select locations of large scenario earthquakes. Figure 3a shows epicenters and projected fault planes of the eight blind-thrust scenario earthquakes considered here.

At each scenario location (Table 1), the modified Northridge slip distribution rupture model is initiated at 5 km depth within each of the basin and nonbasin 3D physical-structure models, congruent with linear clusters of shallow seismicity. Figure 4 shows east–west component time snapshots from 3D basin-model simulations of four selected scenarios. Ⓔ For these four selected scenarios, movies of the simulations and time snapshots of all three components of motion are available in the electronic supplement to this paper; the largest motions generally occur in the north–south and vertical directions related to the predominantly north-dipping thrust-faulting source model. Overall, outward radiating waves are distorted by the presence of the northwest-oriented Georgia basin structure; the highest amplitude shaking occurs near the epicenter and within the basin. Interference between scattered waves within the Georgia basin is apparent late in the simulations. The four selected scenario earthquakes are similar in location and magnitude to scenarios developed by the State of Washington Emergency Management Division for planning purposes (Wood and Ratliff, 2011); hence, future large crustal NA plate earthquakes are considered likely in these locations. These four scenarios are discussed in detail later in this section. Composite results based on all eight scenario earthquakes are discussed in the following section.

For each scenario, Table 2 lists the maximum peak motion and basin amplification values for the three different PGV metrics within the Georgia basin and Greater Vancouver regions, as well as the average maximum PGV of all eight

Table 2
Maximum PGV (cm/s) and Associated Basin Amplification Factor

Scenario	2DgmPGV* (cm/s)	2DrssPGV† (cm/s)	3DrssPGV‡ (cm/s)	2DgmPGV* (Factor)	2DrssPGV† (Factor)	3DrssPGV‡ (Factor)
Georgia Basin Region						
1	110.4	184.5	467.2	9.2	17.8	14.0
2	71.1	104.8	148.4	5.6	5.9	4.3
3	140.0	231.5	376.4	13.9	13.9	7.2
4a	48.7	74.2	209.1	22.4	19.7	19.5
4b	49.2	69.7	188.4	6.7	6.8	5.6
5	44.2	72.7	78.3	13.6	10.0	6.7
6	43.9	66.2	76.5	9.2	6.7	4.6
7	45.3	64.1	69.8	8.4	8.4	6.3
Average (1 standard deviation)	39.8 (36.5)	62.1 (62.8)	83.6 (140.9)	8.1 (5.1)	7.0 (5.0)	5.9 (5.0)
Greater Vancouver Region						
1	15.7	13.4	15.6	4.2	4.2	3.7
2	24.7	35.0	41.7	3.3	3.1	2.5
3	42.1	63.2	46.2	5.5	4.1	2.9
4a	10.6	15.7	17.8	8.9	7.8	6.5
4b	17.7	28.1	32.4	2.6	2.9	2.4
5	14.0	20.8	25.0	3.6	3.6	3.0
6	26.0	37.8	54.2	7.9	4.6	4.4
7	18.9	26.7	28.4	3.8	3.3	2.6
Average (1 standard deviation)	17.8 (9.7)	26.1 (15.4)	31.8 (13.8)	4.1 (2.1)	3.6 (1.5)	2.9 (1.3)

*Geometric mean of two horizontal components.
†Root sum of squares of two horizontal components.
‡Root sum of squares of three components.

scenario earthquakes for each region. The preferred 2DgmPGV values are consistently lower than the root sum of squares metric (2DrssPGV) as expected, especially the 3DrssPGV metric as the vertical component motion is generally higher or of similar amplitude to the horizontal motion due to the thrust-faulting scenarios. Figure 5 shows PGV maps of the preferred 2DgmPGV metric for all eight scenarios; panel layout corresponds to the spatial distribution of the scenario earthquake locations. Ⓔ Figure S3, available in the electronic supplement, shows 3DrssPGV maps for all eight scenarios. Generally, the highest ground motions coincide with the lowest velocity sediments in the upper 1 km of the model, although the level and spatial extent of ground shaking is unique to each scenario. The range in predicted maximum PGV in Greater Vancouver is 11–42 cm/s, which corresponds to modified Mercalli intensities (MMI) VI–VIII; PGV values are converted to modified Mercalli intensity (MMI) estimates here using the relation of Worden *et al.* (2012),

$$\mathrm{MMI} = 2.89 + 3.16\log(\mathrm{PGV}), \qquad (1)$$

which is based on shallow California earthquakes and used for the generation of global earthquake ShakeMaps by the U.S. Geological Survey. Basin and nonbasin synthetic waveforms at 10 selected sites (open squares in Fig. 5) along a 100 km north–south profile that passes through Greater Vancouver are shown in Figure 6. Basin amplification maps (ratio of 2DgmPGV between basin and nonbasin simulations) for the eight scenario earthquakes are shown in Figure 7. Ⓔ Basin amplification maps based on the 3DrssPGV metric for all eight scenarios are shown in Figure S4, available in the electronic supplement. Overall, the amplitude and duration of shaking is increased within the basin; focusing of surface waves in the narrow and deep southeast portion of the basin causes high-amplitude surface waves.

To assess the potential increase in the duration of shaking due to the presence of Georgia basin sediments, the cumulative time of total horizontal motion is determined for three locations in Greater Vancouver (Table 3) using

$$A(t) = \sqrt{a_{\mathrm{EW}}(t)^2 + a_{\mathrm{NS}}(t)^2} \qquad (2)$$

(Tumarkin and Archuleta, 1997). The sum of time periods of a specified threshold level is known as the effective or uniform duration (e.g., Bommer and Martinez-Pereira, 1999). The chosen threshold level is 3.4 cm/s, corresponding to moderate shaking MMI V (Worden *et al.*, 2012).

Scenarios that generate the highest motions (≥25 cm/s) occur 45–80 km south-southwest of Vancouver, that is, scenarios 2, 3, and 6. For scenarios 2 and 3, 45–50 km distant, the high-amplitude shaking in Vancouver is associated with early shear-wave arrivals, whereas for scenario 6 at 80 km distance, PGV is associated with later surface-wave arrivals (Fig. 6). Basin amplification in Greater Vancouver is therefore lower for scenarios 2 and 3 than 6. However, these three scenarios exhibit the longest effective duration of moderate-level shaking (≥3.4 cm/s), an average of 34 s. For all three

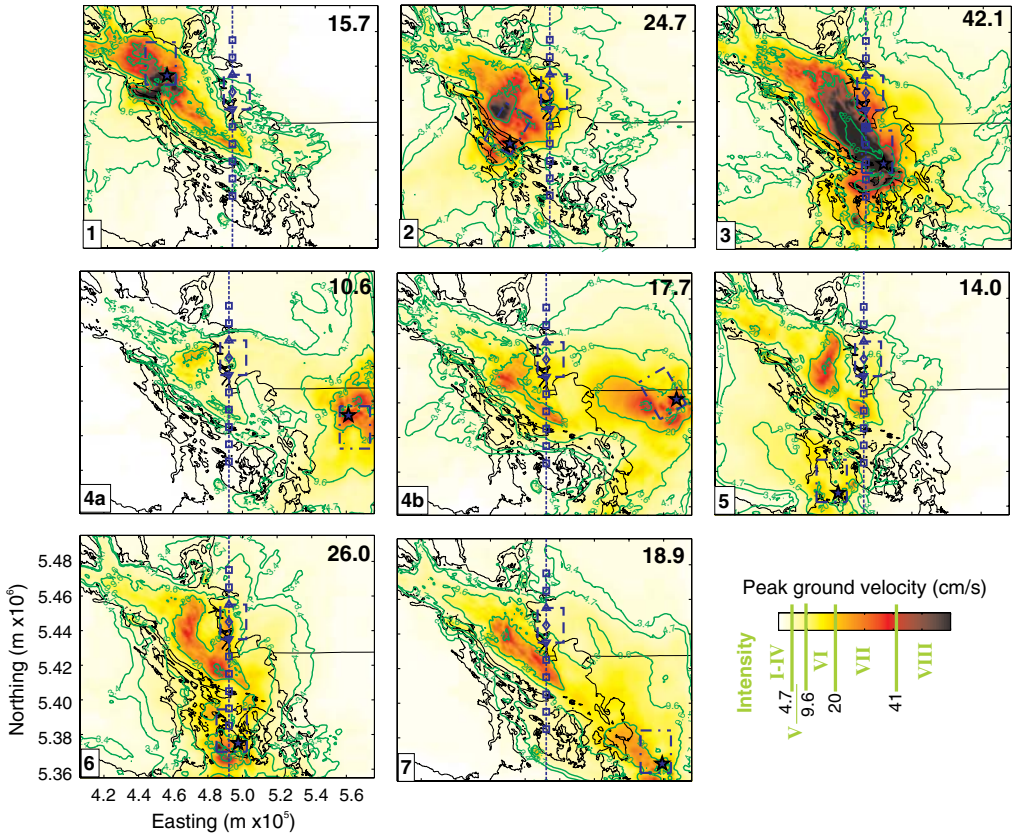

Figure 5. Maps of PGV (cm/s) for all eight scenario earthquakes (contour lines correspond to the MMI intervals of Worden *et al.*, 2012); the projected fault plane and hypocenter are shown by the dotted-dashed box and star, respectively, and the coastline and the international border are shown by the black lines. Numbers in the upper right of each panel correspond to the maximum PGV within Greater Vancouver (dashed rectangle). The squares along the north–south cross section correspond to 10 locations of extracted waveforms (10 km spacing) shown in Figure 6; locations representative of Vancouver (upward triangle), Richmond (diamond), and Ladner (downward triangle) are marked. The color version of this figure is available only in the electronic edition.

scenarios, rupture is directed across the Georgia basin sediments into Vancouver; the highest amplitude surface-wave arrivals occur as waves propagate across the deep southeast part of the basin toward Vancouver (scenarios 3 and 6).

Scenario 1: Georgia Strait Event

A shallow M_w 6.8 blind-thrust scenario earthquake is simulated at the hypocenter of the 1997 M_L 4.6 earthquake beneath northwest Georgia Strait, ~40 km west of Vancouver. The fault plane is oriented according to the 1997 mainshock; an east–west striking north-dipping structure. Rupture propagates down-dip, toward north, based on the temporal aftershock sequence (Cassidy *et al.*, 2000). Outward radiating waves are distorted by the presence of the northwest-oriented Georgia basin structure (Fig. 4). High-amplitude surface waves occur southeast of the epicenter, south of Vancouver, coincident with narrowing and deepening of the basin structure. The highest amplitude shaking occurs near the epicenter and along the northwest-oriented long axis of the basin (Fig. 5). The synthetic waveforms in Figure 6 show the amplitude and duration of shaking is increased within the basin; focusing of the surface waves in the deep southeast portion of the basin causes high-amplitude shaking at 40–50 s, which persists to ~80 s. Across Greater Vancouver, the average PGV is 15.7 cm/s (Table 2), corresponding to strong to very strong shaking MMI VI–VII.

Figure 7 shows the basin amplification map and Figure 8 shows the corresponding synthetic basin and nonbasin modeled synthetic waveforms at three sites spaced 20 km apart across Greater Vancouver, from north to south: Vancouver, Richmond, and Ladner. The highest basin amplification is a factor of 9.2 and occurs in the deep southeast portion of the basin due to the high-amplitude surface waves apparent in the synthetic basin-model waveforms (Fig. 6). Across Greater Vancouver, the average basin amplification factor is 4.2. When Georgia basin sediments are included in the 3D structure model, the duration of moderate (and higher) shaking is 8 and 15 s in Richmond and Ladner, respectively (Table 3), whereas when basin sediments are not included in the velocity model, the duration is 0 s because the level of shaking does not surpass the 3.4 cm/s threshold. In Vancouver, the duration of shaking is increased by the 3D basin structure but is always below the chosen moderate-level threshold for this scenario.

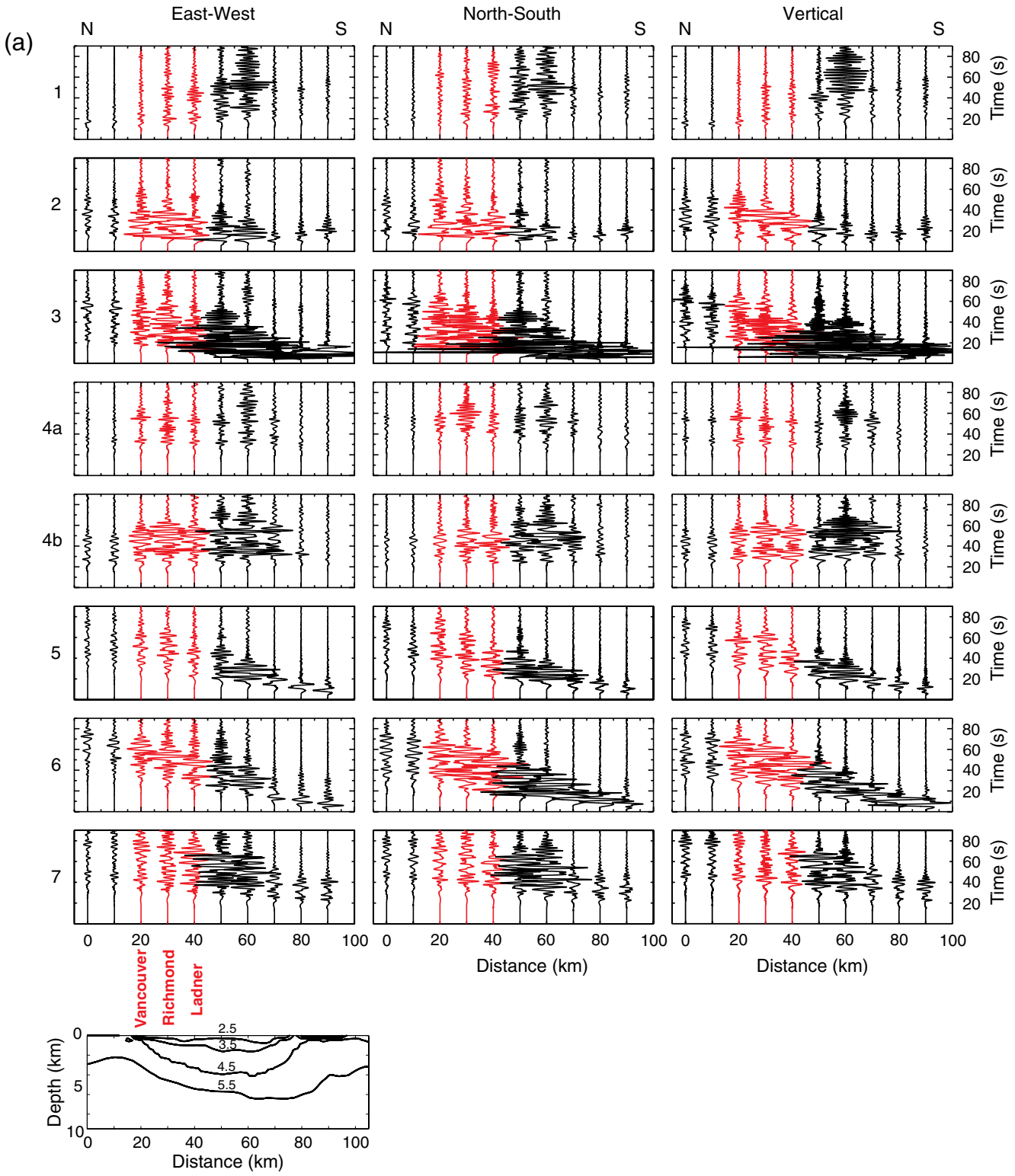

Figure 6. Synthetic (a) basin and (b) nonbasin waveforms for all eight scenario earthquakes along the north–south profile shown in Figure 5. Waveforms corresponding to the cities of Vancouver, Richmond, and Ladner are shown in lighter shade. The bottom panel shows the corresponding north–south cross section of the (a) basin and (b) nonbasin models (contours of V_P [km/s] are labeled) to 10 km depth. The color version of this figure is available only in the electronic edition. (*Continued*)

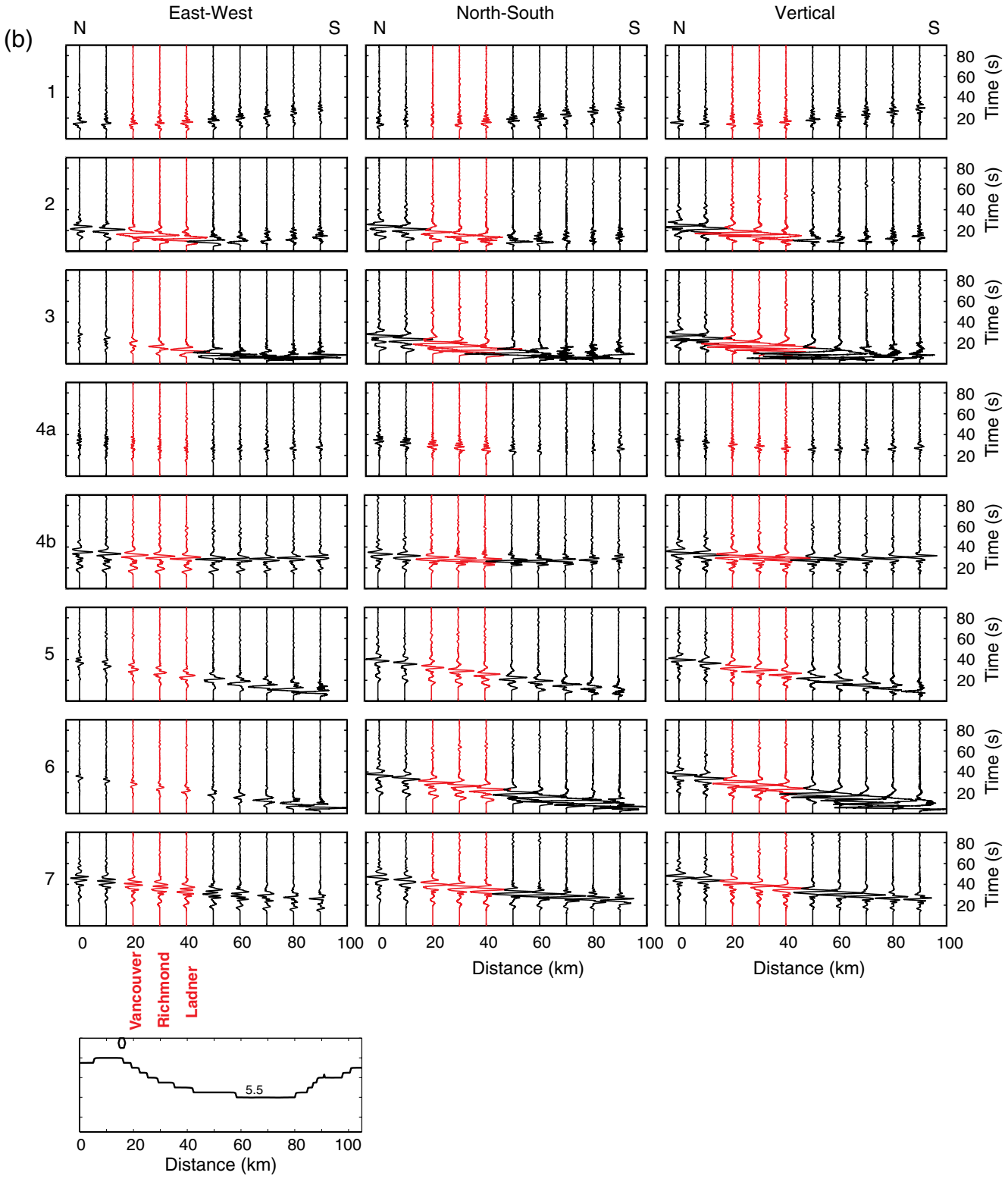

Figure 6. Continued.

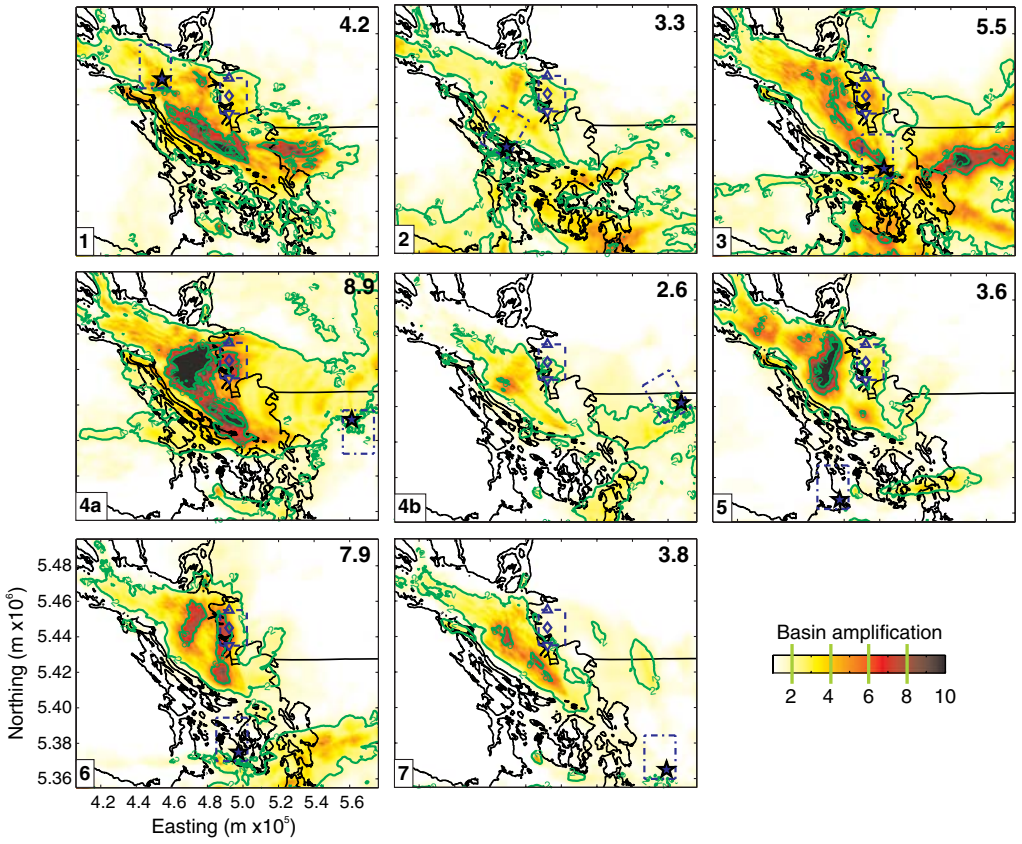

Figure 7. Maps of basin amplification for all eight scenario earthquakes. The projected fault plane and hypocenter are shown by the dotted-dashed box and star, respectively, and the coastline and international border are shown by black lines. Numbers in the upper right of each panel correspond to the maximum basin amplification factor within Greater Vancouver (dashed rectangle); locations of Vancouver (upward triangle), Richmond (diamond), and Ladner (downward triangle) are marked. The color version of this figure is available only in the electronic edition.

Scenario 6: San Juan Island Event

A shallow M_w 6.8 blind-thrust scenario earthquake is simulated beneath San Juan Island, Washington, ~80 km south of Vancouver. Two historical moderate earthquakes occurred in this region in 1909 and 1920. Table 1 provides details of the modified Northridge source model; the hypocenter location is determined by projecting the linear seismic trend at 10–20 km determined by Balfour, Cassidy, and Dosso (2011) to 5 km depth and is similar to the hypocenter of the 1920 M 5.5 event. Propagation of rupture is directed down-dip (north) beneath the deep southeast portion of the Georgia basin and toward Greater Vancouver.

During the first 30 s of the simulation (Fig. 4), radiating wavefronts propagate north into the basin. The synthetic waveforms at 0–40 km distance (Fig. 6) show large amplitude early-arrival shear waves, primarily on the north–south

Table 3
Cumulative Duration (s) of Moderate-Level (≥3.4 cm/s) Shaking

	Vancouver			Richmond			Ladner		
Scenario	Basin Model (s)	Nonbasin Model (s)	Ratio	Basin Model (s)	Nonbasin Model (s)	Ratio	Basin Model (s)	Nonbasin Model (s)	Ratio
1	0.0	0.0	*0.0*	8.0	0.0	*8.0*	15.9	0.0	*15.9*
2	29.0	4.5	6.4	29.4	5.1	5.7	24.7	5.2	4.8
3	39.7	4.7	8.4	43.6	6.1	7.1	35.2	6.7	5.3
4a	6.3	0.0	*6.3*	26.0	0.0	*26.0*	8.1	0.0	*8.1*
4b	20.8	4.3	4.9	32.3	4.6	7.0	29.0	4.8	6.0
5	15.2	1.4	10.9	25.9	2.1	12.3	18.9	1.9	9.9
6	33.2	2.4	13.8	37.2	2.4	15.5	33.8	3.1	10.9
7	18.9	4.2	4.5	35.8	4.7	7.6	34.2	4.9	7.0

Italicized values indicate the basin model duration divided by one, in lieu of nonbasin model zero value.

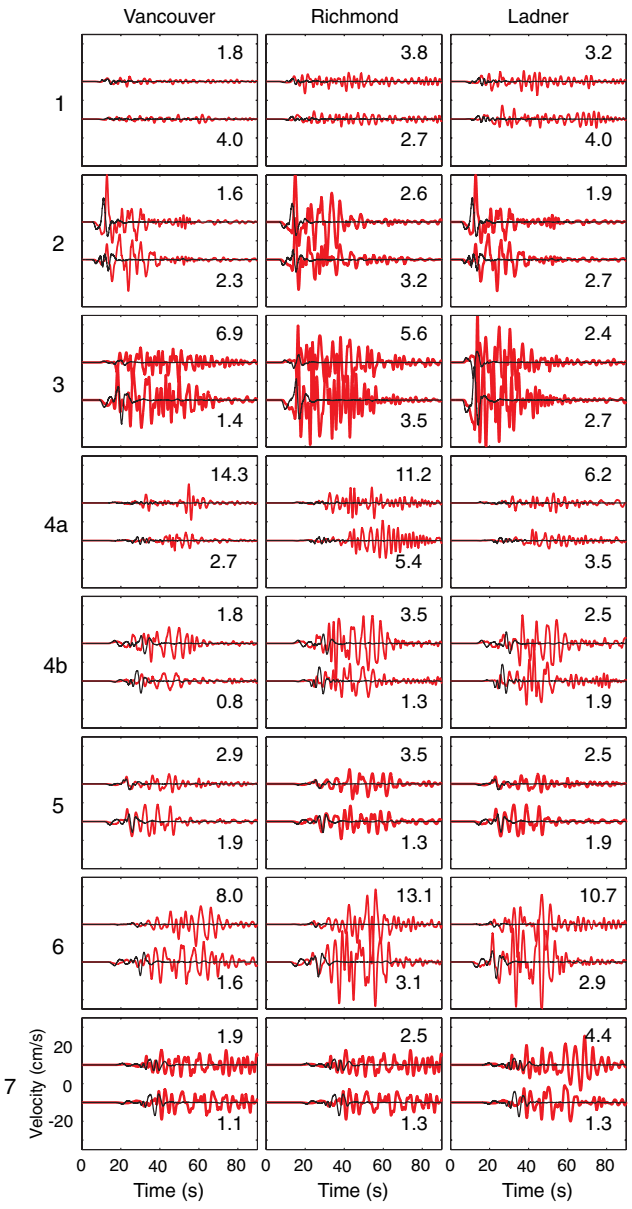

Figure 8. Comparison of east–west (upper) and north–south (lower) waveforms for basin (lighter shade) and nonbasin (black) models at three locations in Greater Vancouver for all eight scenario earthquakes. Numbers in the panels correspond to the associating basin amplification factor. The color version of this figure is available only in the electronic edition.

and vertical components, which are focused at 40 km distance in the deep southeast portion of the basin and significantly increase in amplitude. By 40 s, basin-edge generated surface waves arrive at this midbasin location. At 40–60 s in the simulation, there is an apparent focusing of the surface-wave fronts as they propagate north across Greater Vancouver (Fig. 4), primarily coincident with basin structure of the upper 1 km. For the three sites across Greater Vancouver at 60–80 km distance, the surface-wave arrivals at 40–60 s are of similar and/or larger amplitude than early-arrival shear waves. The constructive interference of surface waves here causes high-amplitude surface waves to propagate north out of the basin, which is apparent at 50 s onward in the simulation (Fig. 4) for the two sites at 90 and 100 km distance (Fig. 6). At 60–80 s in the simulation, interference between scattered waves within the Georgia basin is apparent. Overall, the highest amplitude shaking occurs near the epicenter, in the deep southeast portion of the basin, and along and offshore west Greater Vancouver (Fig. 7) from focusing of surface waves propagating north out of the deep southeast portion of the basin coincident with the lowest-velocity basin sediments present in the upper 1 km. The average PGV across Greater Vancouver is 26.0 cm/s (Table 2), equivalent to a very strong shaking MMI VII.

The highest basin amplification is a factor of 7.9 and occurs in zones west and south offshore Vancouver (Fig. 6). Across Greater Vancouver, the average basin amplification factor is 7.9. High-amplitude late-arriving surface waves are apparent for both horizontal components of motion (Fig. 6); however, the amplification factor is significantly higher for east–west component waveforms due to minimal source directivity (Fig. 8). The effective duration of moderate-level shaking is 33–37 s in Greater Vancouver (Table 3), an increase of 11–15 times the duration of the nonbasin waveforms.

Scenarios 4a and 4b: Deming, Washington, Events

The 1990 shallow earthquake sequence near Deming, Washington, ~80 km east-southeast of Vancouver, initially occurred in a southeast-dipping linear manner; after four days, shallow events occurred in a northwest-dipping linear manner (Amadi, 1992; Dragovich *et al.*, 1997). These two possible rupture orientations are investigated here as potential large shallow earthquake scenarios: scenario 4a is characterized by a N90°E striking 45° south-dipping thrust plane (because a southeast-dipping thrust plane could not be accommodated within the physical-structure models), and scenario 4b is characterized by a N240°E striking 45° northwest-dipping thrust event.

Time snapshots of the two scenario simulations are generally similar (Fig. 4). The radiating wavefront is nearly planar as it enters the basin along its east margin; early shear-wave arrivals occur simultaneously at ~25–30 s for all sites along the north–south profile (Fig. 6). During the next 10 s, amplitudes of early shear-wave arrivals are comparatively low or high for scenarios 4a and 4b, respectively, depending on the directivity of the source. At 40–60s, constructive interference of the east-propagating shear waves with waves generated along the margins of the northwest-oriented basin occurs resulting in the highest levels of shaking.

Similar strong levels of shaking result from the two scenarios with average maximum PGV of 10.6 cm/s (MMI VI) and 17.7 cm/s (MMI VII) across Greater Vancouver for scenarios 4a and 4b, respectively (Table 2). In contrast, the average maximum 3D basin amplification across Greater Vancouver (Fig. 7) is significantly larger for scenario 4b than scenario 4a (factors of 8.9 and 2.6, respectively). This large

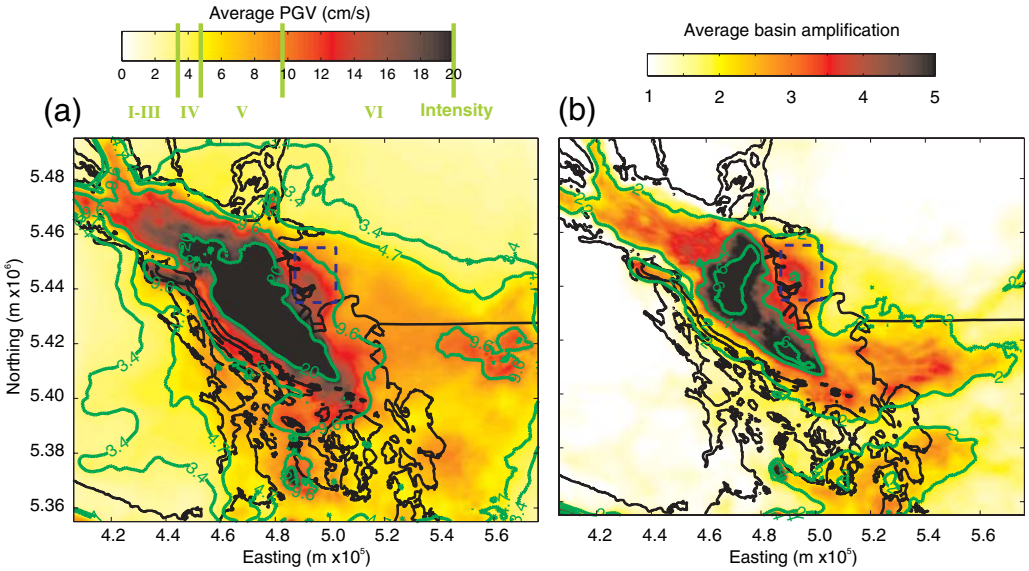

Figure 9. (a) Average PGV and (b) basin amplification for all eight scenario earthquakes. The solid line denotes coastline and the international border; the dashed box outlines Greater Vancouver. The color version of this figure is available only in the electronic edition.

difference in predicted basin amplification is related to the amplitude of the nonbasin waveforms; for scenario 4a, the source is directed south away from Greater Vancouver resulting in low-amplitude nonbasin waveforms and high basin amplification values, particularly for the east–west component of motion (Fig. 8). The effective duration of moderate-level shaking (Table 3) is 6–12 s longer for scenario 4b than scenario 4a. Overall, scenario 4b results in 1.7 times higher peak motion on average, and up to 3.5 times longer shaking than scenario 4a, in which thrust motion is directed northwest beneath Greater Vancouver rather than south away from the city, respectively.

Composite Results

This section compares results of the eight scenarios considered in this study. Figure 9 presents maps of the average PGV and basin amplification for all eight scenarios. The presence of the Georgia basin significantly increases the level of predicted long-period ground motions. For the Georgia basin region as a whole, the average maximum PGV is 39.8 cm/s, equivalent to very strong to severe shaking MMI VIII–IX. The average maximum basin amplification is a factor of 8.0 within the Georgia basin region. More importantly, in the onshore Greater Vancouver region, the average maximum peak motion is 17.8 cm/s. Therefore, on average, the predicted intensity of shaking at stiff soil sites in Greater Vancouver for an M_w 6.8 shallow blind-thrust earthquake corresponds to very strong shaking MMI VII. The basin structure model does not include soft sediments (V_S < 625 m/s) or surface topography which may also amplify ground shaking. For reference, long-period horizontal PGV of the M_w 6.7 Northridge earthquake generally exceeds 20 cm/s (MMI VII) in the Los Angeles basin, associated with U.S. $41.8 billon in damage (rupture propagated upward, rather than the downward propagation considered here). The average maximum increase in peak motion due to basin structure in Greater Vancouver is a factor of 4.1. The average effective duration of moderate-level shaking increases from 3 s without basin sediments to 25 s when Georgia basin sediments are included in the 3D structure model.

The proposed predictor variable for basin amplification is the depth to either a V_S of 1.0 ($Z_{1.0}$), 1.5 ($Z_{1.5}$), or 2.5 ($Z_{2.5}$) km/s, with $Z_{1.5}$ preferred for the Los Angeles basin (Day *et al.*, 2008). Figure 10 shows that the area of moderate and higher basin amplification (≥2) is primarily associated with near-surface low-velocity sediments ($Z_{1.0}$ of 250 m or $Z_{1.5}$ of 500 m) and is not associated with higher-velocity sediments at greater depth ($Z_{2.5}$). The appropriate measure of basin amplification for the Georgia basin appears to be $Z_{1.0}$ or $Z_{1.5}$, but not $Z_{2.5}$, as was also determined for deep JdF plate scenario earthquakes (Molnar *et al.*, 2014). Hence, ground-motion prediction equations that include a basin sediment-thickness correction term based on $Z_{2.5}$ are less appropriate for use here than those based on $Z_{1.0}$ or $Z_{1.5}$.

Comparison of Shallow and Deep M_w 6.8 Scenario Earthquakes

Finite-difference simulations of shallow (5 km) NA plate earthquakes are presented here, whereas simulation of deep (42–55 km) JdF plate earthquakes are considered in Molnar *et al.* (2014). For both shallow and deep scenario earthquakes, the same moment magnitude is used, and the entire rupture process takes 10 s; however, the rupture model varies from a normal-faulting point source (potency of 0.3 km^3) for deep scenarios to a distributed slip blind-thrust fault source (potency of 0.7 km^3) for shallow scenarios.

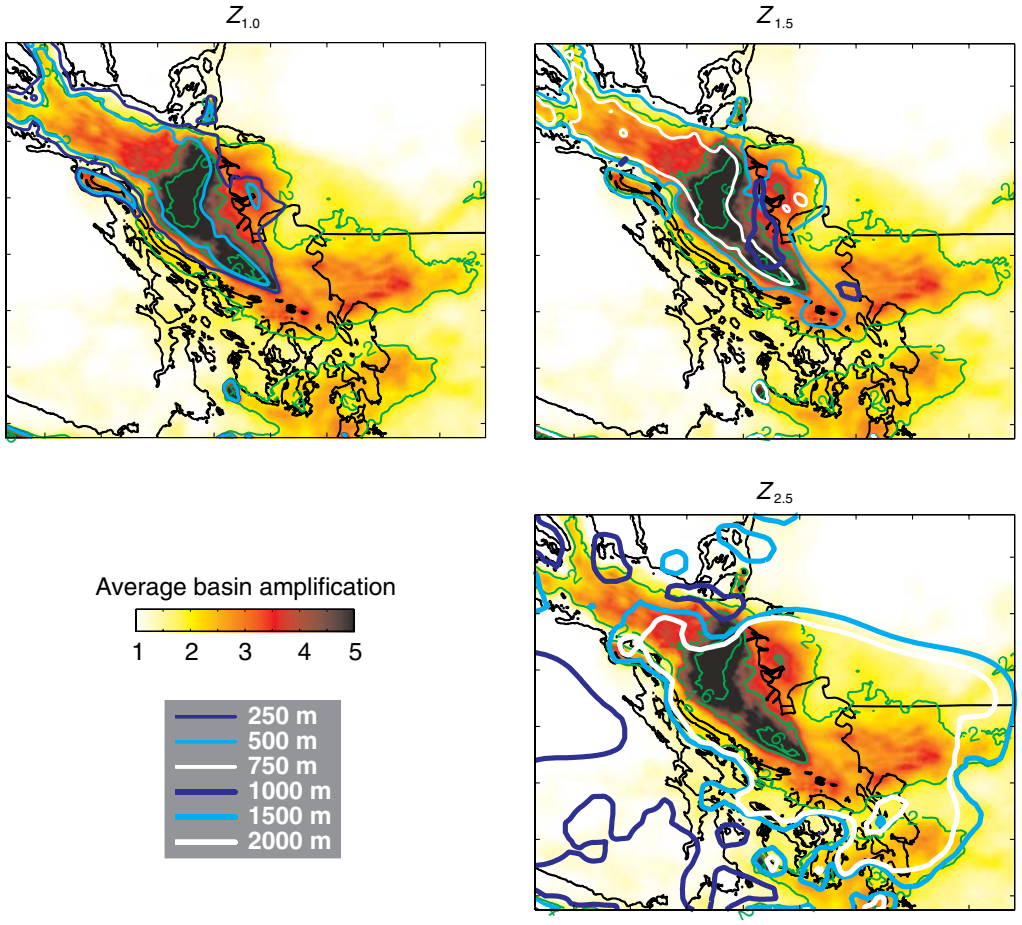

Figure 10. Average basin amplification compared to $Z_{1.0}$, $Z_{1.5}$, and $Z_{2.5}$ isodepth contours in the upper 2 km of the basin model. The coastline and international border are shown by thin black lines. The color version of this figure is available only in the electronic edition.

Average peak ground motion and basin amplification levels within Greater Vancouver are higher for shallow sources, as expected: 17.8 cm/s (MMI VII) and factor of 4.1 compared with 3.2 cm/s (MMI IV–V) and factor of 3.1. However, the ground-motion distribution generally spans a larger area for shallow scenarios than deep scenarios; higher-amplitude shaking from shallower sources excites the entire Georgia basin structure (Fig. 9), whereas lower-amplitude shaking from deeper sources predominantly excites narrow and deep portions of the basin (fig. 12 in Molnar *et al.*, 2014).

Shallow and deep scenario earthquakes with similar epicenters occur in two cases; Figure 11 compares both shallow and deep basin-model waveforms along the 100 km north–south profile through Greater Vancouver for the two comparable epicenters 40 km west and 80 km south of Vancouver. There are two general similarities: (1) the timing of first arrivals is similar along the profile, in which first arrivals are delayed with increasing distance from the epicenter and occur later for deep sources in the near-source region, and (2) the amplitude of late-arriving surface waves is higher for the southern shallow and deep sources. This latter observation is a significant contribution to the understanding of earthquake ground shaking in southwest British Columbia; the presence of the northwest-oriented Georgia basin significantly amplifies ground motions in Greater Vancouver for scenario earthquakes that are oriented south-southwest of the city and occur on the distal side of the Georgia basin ($\geq$50 km distant).

Conclusions

To assess the effects of 3D Georgia basin structure on long-period ($>$2 s) ground motion due to large shallow earthquakes within 100 km of Greater Vancouver, numerical 3D FD modeling of viscoelastic wave propagation is carried out. This research provides the first detailed investigation of 3D earthquake ground motion for a sedimentary basin in Canada. Shorter period ground motions are not resolved, limited by the grid spacing and minimum V_S chosen for the 3D basin model according to a $\geq$5 node per minimum shear wavelength rule-of-thumb commonly used for fourth-order FD schemes. Overall the work presented here (and in Molnar *et al.*, 2014) represents an important step toward quantifying the effect of the Georgia basin on earthquake ground motion in southwest British Columbia.

A total of eight shallow blind-thrust scenario earthquakes within the overriding NA plate are simulated on potential

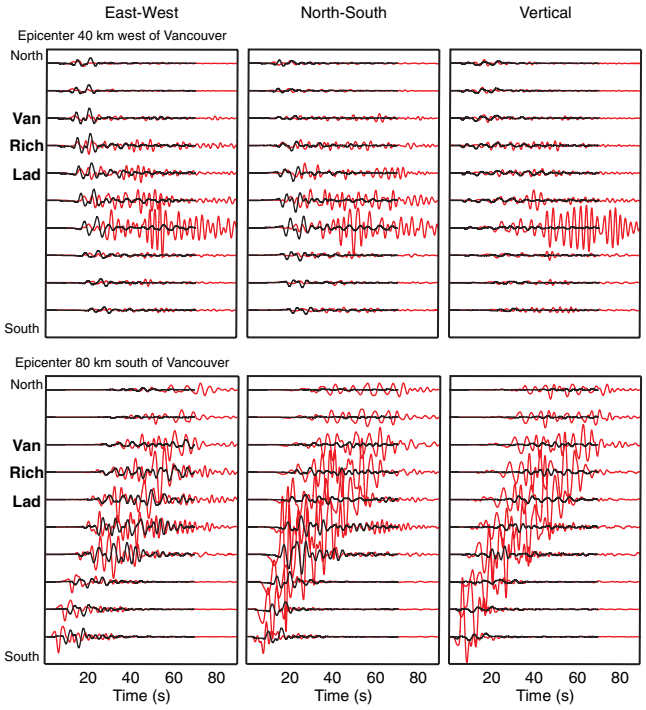

Figure 11. Waveforms generated along the north–south profile through Greater Vancouver in Figure 5 from simulation of deep normal-faulting (black) and shallow blind-thrust (light shade) events with similar epicenters. The color version of this figure is available only in the electronic edition.

active faults with hypocenters in locations of linear clustered seismicity. All simulated earthquakes are characterized by a single slip distribution model based on the blind-thrust rupture of the M_w 6.7 Northridge earthquake. Nonetheless, the FD simulations presented here provide significant insight to the expected amplification in ground shaking due to 3D basin structure. For all simulations, some general effects are observed consistently when Georgia basin sediments ($625\ \text{m/s} \le V_P < 5.5\ \text{km/s}$) are included in the 3D structure model. The symmetry of the seismic radiation pattern is distorted, and the area of higher ground motions is increased. Surface waves are generated in the southeast and northwest parts of the basin coincident with steep basin edges in the upper 1 km of the model. The average maximum peak ground motion for a shallow M_w 6.8 blind-thrust NA plate earthquake in the Georgia basin model is 39.8 cm/s (MMI VIII–IX), and the average maximum basin amplification factor is 8; for the Greater Vancouver region, the average maximum PGV and basin amplification is 17.8 cm/s (MMI VII) and a factor of 4.1, respectively. Overall, the highest basin amplification (largest surface waves) generated across Greater Vancouver is associated with shallow earthquakes located $\ge$50 km south-southwest of the city. The area of basin-amplified motion ($\ge$4) is primarily associated with the lowest-velocity sediments at $<$750 m depth of the 3D basin model.

The work presented here and in Molnar *et al.* (2014) is a first step in understanding the influence of the 3D Georgia basin structure to the long-period ground motion in Greater Vancouver. Conclusions are drawn from a limited number of simulations that are specific to the chosen earthquake locations and single pure blind-thrust rupture style. The rupture characteristics of large shallow earthquakes are more complex and less constrained than for large deep earthquakes in southwest British Columbia, such that conclusions drawn here are not as robust as for deep scenario events presented in Molnar *et al.* (2014). Overall, the results of this work and Molnar *et al.* (2014) show that the presence of the 3D Georgia basin structure increases the level and duration of predicted long-period ground motion in Greater Vancouver for large scenario earthquakes in southwest British Columbia.

Data and Resources

Subvolumes of the Pacific Northwest Community Velocity Model (v1.3) of Stephenson (2007) are used for the 3D modeling. The Anelastic Wave Propagation-Olsen Day Cui (AWP-ODC) finite-difference simulation code was used for the 3D simulations. Maps and time snapshots of FD simulations were generated using MATLAB (MathWorks) software; coordinates of the North American coastline were obtained at http://www.ngdc.noaa.gov/mgg/coast/ (last accessed August 2010). Waveforms were filtered and plotted using Seismic Analysis Code (Incorporated Research Institutions for Seismology) software.

Acknowledgments

The authors gratefully acknowledge beneficial discussions with Garry Rogers (NRCAN, Pacific), Patrick Monahan (Penn West Exploration), Art Frankel (USGS, Washington), and Arben Pitarka (URS, California). Thank you to Robert Kung (NRCAN, Pacific) for GIS support, and Minerva computer support staff at the University of Victoria. We gratefully acknowledge reviews by Allison Bent (NRCAN, Ottawa) and two anonymous reviewers. Funding provided by National Sciences and Engineering Research Council (NSERC) of Canada, University of Victoria, and Natural Resources Canada. This is ESS Contribution 20130063.

References

Aagaard, B. T., T. M. Brocher, D. Dolenc, D. Dreger, R. W. Graves, S. Harmsen, S. Hartzell, S. Larsen, K. McCandless, S. Nilsson, N. A. Petersson, A. Rodgers, B. Sjögreen, and M. L. Zoback (2008). Ground-motion modeling of the 1906 San Francisco earthquake, Part II: Ground-motion estimates for the 1906 earthquake and scenario events, *Bull. Seismol. Soc. Am.* **98,** 1012–1046.

Aagaard, B. T., R. W. Graves, A. Rodgers, T. M. Brocher, R. W. Simpson, D. Dreger, N. A. Petersson, S. C. Larsen, S. Ma, and R. C. Jachens (2010). Ground-motion modeling of the Hayward fault scenario earthquakes, Part II: Simulation of long-period and broadband ground motions, *Bull. Seismol. Soc. Am.* **100,** 2945–2977.

Adams, J. A., and S. Halchuk (2003). Fourth generation seismic hazard maps of Canada: Values for over 650 Canadian localities intended for the 2005 National Building Code of Canada, *Geol. Surv. Canada Open-File Rept. 4459*, 155 pp.

Amadi, E. E. (1992). The 1990 Noonsack Forks, Washington, earthquake sequence: Sequence geometry and temporal characteristics, *M.S. Thesis*, Boise State University, Boise, Idaho, 103 pp.

Avouac, J., F. Ayoub, S. Leprince, O. Konca, and D. V. Helmberger (2006). The 2005, M_w 7.6 Kashmir earthquake: Sub-pixel correlation of ASTER images and seismic waveforms analysis, *Earth Planet. Sci. Lett.* **249,** 514–528.

Balfour, N. J., J. F. Cassidy, and S. E. Dosso (2011). Identifying active structures using double-difference earthquake relocations in southwest British Columbia and the San Juan Islands, Washington, *Bull. Seismol. Soc. Am.* **102,** 639–649.

Balfour, N. J., J. F. Cassidy, S. E. Dosso, and S. Mazzotti (2011). Mapping crustal stress and strain in southwest British Columbia, *J. Geophys. Res.* **116,** no. B03314, doi: 10.1029/2010JB008003.

Bommer, J. J., and A. Martinez-Pereira (1999). The effective duration of earthquake strong motion, *J. Earthq. Eng.* **3,** 127–172.

Cassidy, J. F., G. C. Rogers, and F. A. Waldhauser (2000). Characterization of active faulting beneath the Strait of Georgia, British Columbia, *Bull. Seismol. Soc. Am.* **90,** 1188–1199.

Collino, F., and C. Tsogka (2001). Application of the PML absorbing layer model to the linear elastodynamic problem in anisotropic heterogeneous media, *Geophysics* **66,** 294–307.

Day, S. M., R. Graves, J. Bielak, D. Dreger, S. Larsen, K. B. Olsen, A. Pitarka, and L. Ramirez-Guzman (2008). Model for basin effects on long-period response spectra in southern California, *Earthq. Spectra* **24,** 257–277.

Dragovich, J. D., J. E. Zollweg, A. I. Qamar, and D. K. Norman (1997). The Macaulay Creek thrust, the 1990 5.2-magnitude Deming earthquake, and Quaternary geologic anomalies in the Deming area, western Whatcom County, Washington: Cause and effects? *Wash. Geol.* **25,** 15–27.

Frankel, A. D., W. Stephenson, and D. Carver (2009). Sedimentary basin effects in Seattle, Washington: Ground-motion observations and 3D simulations, *Bull. Seismol. Soc. Am.* **99,** 1579–1611.

Graves, R. W., and A. Pitarka (2004). Broadband time history simulation using a hybrid approach, in *Proc. 13th World Conference on Earthquake Engineering*, Vancouver, British Columbia, 1–6 August 2004, Paper 1098.

Harmsen, S., S. Hartzell, and P. Liu (2008). Simulated ground motion in Santa Clara Valley, California, and vicinity from M 6.7 scenario earthquakes, *Bull. Seismol. Soc. Am.* **98,** 1243–1271.

Hartzell, S., A. Frankel, P. Liu, Y. Zeng, and S. Rahman (2011). Model and parametric uncertainty in source-based kinematic models of earthquake ground motion, *Bull. Seismol. Soc. Am.* **101,** 2431–2452.

Heaton, T. H. (1990). Evidence for and implications of self-healing pulses of slip in earthquake rupture, *Phys. Earth Planet. In.* **64,** 1–20.

Marcinkovich, C., and K. Olsen (2003). On the implementation of perfectly matched layers in a three-dimensional fourth-order velocity-stress finite difference scheme, *J. Geophys. Res.* **108,** no. B5, doi: 10.1029/2002JB002235.

Molnar, S., J. F. Cassidy, K. B. Olsen, S. E. Dosso, and J. He (2014). Earthquake ground motion and 3D Georgia basin amplification in SW British Columbia: Deep Juan de Fuca plate scenario earthquakes, *Bull. Seismol. Soc. Am.* **104,** no. 1, doi: 10.1785/0120110277.

Olsen, K. B. (1994) Simulation of three-dimensional wave propagation in the Salt Lake Basin, *Ph.D. Thesis*, University of Utah, Salt Lake City, Utah, 157 pp.

Olsen, K. B. (2000). Site amplification in the Los Angeles basin from three dimensional modeling of ground motion, *Bull. Seismol. Soc. Am.* **90,** S77–S94.

Olsen, K. B., and R. J. Archuleta (1996). Three-dimensional simulation of earthquakes on the Los Angeles fault system, *Bull. Seismol. Soc. Am.* **86,** 575–596.

Olsen, K. B., S. M. Day, L. A. Dalguer, J. Mayhew, Y. Cui, J. Zhu, V. M. Cruz-Atienza, D. Roten, P. Maechling, T. H. Jordan, D. Okaya, and A. Chourasia (2009). ShakeOut-D: Ground motion estimates using an ensemble of large earthquakes on the southern San Andreas fault with spontaneous rupture propagation, *Geophys. Res. Lett.* **36,** L04303, doi: 10.1029/2008GL036832.

Olsen, K. B., S. M. Day, J. B. Minster, Y. Cui, A. Chourasia, D. Okaya, P. Maechling, and T. Jordan (2008). TeraShake2: Spontaneous rupture simulations of M_w 7.7 earthquakes on the southern San Andreas fault, *Bull Seismol. Soc. Am.* **98,** 1162–1185.

Risk Management Solutions (RMS) (2004). The Northridge, California, earthquake, RMS, 10-year retrospective, Newark, California, Revised May 13, 2004, 12 pp., https://support.rms.com/publications/northridgeeq_retro.pdf (last accessed November 2013).

Rogers, G. C. (1979). Earthquake fault plane solutions near Vancouver Island, *Can. J. Earth. Sci.* **16,** 523–531.

Rogers, G. C. (1998). Earthquakes and earthquake hazard in the Vancouver area, in *Geology and Natural Hazards of the Fraser River Delta, British Columbia*, J. J. Clague, J. L. Luternauer, and D. C. Mosher (Editors), Geological Survey of Canada, Bulletin, Vol. 525, 17–25.

Sommerville, P., K. Irikura, R. Graves, S. Sawada, D. Wald, N. Abrahamson, Y. Iwasaki, T. Kagawa, N. Smith, and A. Kowada (1999). Characterizing crustal earthquake slip models for the prediction of strong ground motion, *Seismol. Res. Lett.* **70,** 59–80.

Stephenson, W. J. (2007). Velocity and density models incorporating the Cascadia subduction zone for 3D earthquake ground motion simulations, version 1.3, *U.S. Geol. Surv. Open-File Rept. 2007-1348*, 24 pp.

Tumarkin, A. G., and R. J. Archuleta (1997). Recent advances in prediction and processing of strong ground motions, *Nat. Hazards* **15,** 199–215.

Wald, D. J., T. H. Heaton, and K. W. Hudnut (1996). Rupture history of the 1994 Northridge, California earthquake from strong-motion, GPS, and leveling data, *Bull. Seismol. Soc. Am.* **86,** S49–S70.

Wood, N., and J. Ratliff (2011). Population and business exposure to twenty scenario earthquakes in the State of Washington, *U.S. Dept. Interior and U.S. Geol. Surv. Open-File Rept. 2011-1016*, 13 pp.

Worden, C. B., M. C. Gerstenberger, D. A. Rhoades, and D. J. Wald (2012). Probabilistic relationships between ground-motion parameters and modified Mercalli intensity in California, *Bull. Seismol. Soc. Am.* **102,** 204–221.

University of Victoria
School of Earth and Ocean Sciences
3800 Finnerty Road
Victoria, British Columbia V8P 5C2
smolnar@uvic.ca
sdosso@uvic.ca
(S.M., S.E.D.)

Natural Resources Canada
P.O. Box 6000
Sidney, British Columbia V8L 4B2
jcassidy@nrcan.gc.ca
jhe@nrcan.gc.ca
(J.F.C., J.H.)

San Diego State University
Department Geological Sciences, GMCS 231A
5500 Campanile Dr
San Diego, California 92182-1020
kbolsen@mail.sdsu.edu
(K.B.O.)

Manuscript received 9 May 2013;
Published Online 21 January 2014